POLITECNICO DI TORINO
Repository ISTITUZIONALE

Are manufacturing I-V Mismatch and Reverse Currents Key Factors in Large Photovoltaic Arrays?

(Article begins on next page)

10 April 2024

Are Manufacturing I–V Mismatch and Reverse Currents Key Factors in Large Photovoltaic Arrays?

Filippo Spertino, *Member, IEEE*, and Jean Sumaili Akilimali

Abstract—In this paper, two factors typical of large photovoltaic (PV) arrays are investigated: one is the current–voltage (I–V) mismatch consequent to the production tolerance; the other is the impact of reverse currents in different operating conditions. Concerning the manufacturing I–V mismatch, the parameters of the equivalent circuit of the solar cell are computed for several PV modules from flash reports provided by the manufacturers. The corresponding I–V characteristic of every module is used to evaluate the behavior of different strings and the interaction among the strings connected for composing PV arrays. Two real crystalline silicon PV systems of 8 × 250 kW and 20 kW are studied, respectively. The simulation results reveal that the impact of the I–V mismatch is negligible with the usual tolerance, and the insertion of the blocking diodes against reverse currents can be avoided with crystalline silicon technology. On the other hand, the experimental results on I–V characteristics of the aforementioned arrays put into evidence the existence of a remarkable power deviation (3%–4%) with respect to the rated power, linkable to the lack of measurement uncertainty in the manufacturer flash reports.

Index Terms—Blocking diodes, equivalent-circuit parameters, manufacturing I–V mismatch, photovoltaic (PV) array, PV module, reverse current.

I. INTRODUCTION

IN RECENT years, significant photovoltaic (PV) deployment has occurred, particularly in Germany (more than 5000 MW installed), Japan (about 2000 MW), and Spain (above 3000 MW), with different configurations. In the first and third cases, a suitable incentive, "feed-in tariff," has driven the job development in terms of manufacturers and installers, while in the second case, funds for research and development and incentives on capital costs have allowed the birth of a market, mainly in the building sector. In the last year, also in Italy, the feed-in tariff has created a good market with volume higher than 100 MW/year. Hence, in many applications, the size of megawatts or tens of megawatts for PV plants is normal today.

Focusing the attention on centralized PV systems in grid connection, there are two relevant factors which can bring significant impacts on large arrays and raise key technical questions:

1) the deviation from the rated power of the individual modules and the mismatch of the current–voltage (I–V)

characteristics for several modules; to what extent the manufacturing I–V mismatch impacts on the maximum power of the whole array?
2) the effect of blocking diodes and/or fuses against reverse currents into several strings with series connected modules; is it profitable to use blocking diodes and/or fuses to prevent reverse currents in multistring plants?

This paper addresses these two issues presenting simulations and experimental results concerning two PV systems of different sizes (2 MW versus 20 kW) and technology (recent modules versus modules installed some years ago). Such PV generators are connected by dc–ac converter (inverter) with maximum power point (MPP) tracker [1]–[8] and a 50-Hz transformer to the medium- and low-voltage grids, respectively.

Other factors of losses in the PV arrays, such as over temperature, dirt, glass reflection, spectral mismatch, voltage drop on the cables, and so forth, assume about identical impact in low-power as well as in high-power ranges. Yet, the I–V mismatch depends on tolerance: in the last ten years, the manufacturers of PV modules have refined the production by reducing the power tolerance from ±10% down to ±3% or less in particular cases (it is worth noting that current and voltage parameters can have higher tolerance). Furthermore, the manufacturer provides the three typical points of the rated I–V characteristic (short-circuit current, open-circuit voltage, and maximum power with its corresponding current and voltage), but the tolerance is given only for maximum power. Then, for every module of the batch, the "flash tests" report the previous parameters *without indicating the measurement uncertainty*. These nameplate data are referred to the standard test conditions (STC) (solar irradiance $G = 1000$ W/m^2 with spectrum AM = 1.5 and cell temperature $T_c = 25\,°C$) and are obtained by "sun simulators" in a dark room.

If the tolerance is ±10%, it is very likely that deviations from rated power and I–V mismatch have a remarkable impact (3%–5%), particularly on PV arrays characterized by thousands of modules; but with ±3% tolerance, it is not simple to estimate "*a priori*" the corresponding impact of I–V mismatch.

II. PV MODELS FOR I–V CURVE SIMULATION

The equivalent circuit of a solar cell with its parameters is a tool to simulate, for whatever irradiance and temperature conditions, the I–V characteristics of each PV module within a batch that will constitute an array of parallel-connected strings of series-connected modules.

With this aim, the literature gives two typical equivalent circuits, in which a current source I_{ph} simulates the photovoltaic
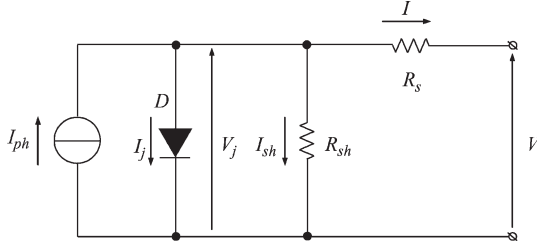
Fig. 1.   Equivalent circuit of solar cell with one exponential.

effect [4], [5], [9]–[13]. One circuit is based on a single exponential model for the p-n junction, in which the reverse saturation current I_o and the quality factor of junction m are the diode parameters to be determined

$$I_j = I_o \cdot \left(e^{\frac{qV_j}{mkT_c}} - 1 \right) \tag{1}$$

where V_j is the junction voltage, k is the Boltzmann constant, q is the electron charge, and T_c is the cell temperature.

The other model involves a couple of exponential terms, in which the quality factors assume fixed values m_1 and m_2, respectively, whereas I_{o1} and I_{o2} must be inserted

$$I_j = I_{o1} \cdot \left(e^{\frac{qV_j}{m_1kT_c}} - 1 \right) + I_{o2} \cdot \left(e^{\frac{qV_j}{m_2kT_c}} - 1 \right). \tag{2}$$

The model with a single exponential is used in this paper (Fig. 1). In this model, the series resistance R_s accounts for the voltage drop in the bulk semiconductor, electrodes, and contacts, and the shunt resistance R_{sh} represents the lost current in the surface paths. Thus, five parameters are sufficient to determine the behavior of the solar cell, namely, the current source I_{ph}, the saturation current I_o, the junction quality factor m, the series resistance R_s, and the shunt resistance R_{sh}. Furthermore, a capacitive parameter has to be inserted to address the dynamic behavior [14].

If we examine the silicon technologies, monocrystalline (m-Si), polycrystalline (p-Si), and amorphous (a-Si), the shape of the $I–V$ curve is mainly determined by the values of R_s and R_{sh}.

With low series resistance and high shunt resistance, the $I–V$ characteristic is close to two perpendicular lines, while with high series resistance and low shunt resistance, the shape is close to a straight line.

Let us consider the $I–V$ curve of the following items:

1) short-circuit current I_{sc};
2) open-circuit voltage V_{oc};
3) current at maximum power I_{MPP};
4) voltage at maximum power V_{MPP};
5) maximum power $P_M = V_{MPP} \cdot I_{MPP}$.

Therefore, a suitable coefficient, i.e., the fill factor $FF = P_M/(V_{oc} \cdot I_{sc})$, distinguishes crystalline silicon (0.70–0.80) from amorphous silicon (0.55–0.65).

With the equivalent circuit of the solar cell, it is possible to obtain the $I–V$ characteristic of the PV module by simply multiplying the voltage by the number of series-connected cells.

In order to study the $I–V$ mismatch with several modules and the generation of reverse current with several parallel-connected strings, the $I–V$ curve can be divided into two parts, in which the behavior is considered to be linear (the "piecewise linear approximation"). In the first part, from the short-circuit point to the MPP, a PV generator (module, string, or array) can be seen in terms of the Norton's theorem as an ideal current source providing I_{sc} with a parallel resistance

$$R_p = \frac{V_{MPP}}{I_{sc} - I_{MPP}}. \tag{3}$$

The second part, from the MPP to the open-circuit point, can be seen in terms of the Thévenin's theorem as a voltage source generating V_{oc} with an internal resistance

$$R_i = \frac{V_{oc} - V_{MPP}}{I_{MPP}}. \tag{4}$$

In the following sections, a simulation approach is presented with the aim of evaluating the amount of mismatch losses and the maximum value of the reverse current by considering, at first, the piecewise linear approximation and, afterward, the fully nonlinear model.

III. EVALUATION OF MANUFACTURING MISMATCH

As well known, the typical structure of an array includes the parallel connection of N_p strings composed of N_s series-connected modules. Hence, the total number of modules is $N_m = N_p \cdot N_s$. By connecting N_m modules to form an array, the maximum power of the array is lower than the summation of the maximum power of every module [15]–[20].

On the basis of the flash reports, this reduction, which is due to an intrinsic $I–V$ mismatch, is expressed as relative power losses $\ell_{mis}^{(array)}$ (positive sign)

$$\ell_{mis}^{(array)} = \frac{\sum\limits_{i=1}^{N_m} \left(P_M^{(i)} \right) - P_M^{(array)}}{\sum\limits_{i=1}^{N_m} P_M^{(i)}} \tag{5}$$

where $P_M^{(i)}$ is the maximum power of the ith module (from flash tests) before the connection with the other modules, and $P_M^{(array)}$ is the actual maximum power on the resulting $I–V$ characteristic after the array connection. Moreover, taking into account that the range of maximum power for all the modules is expressed in terms of $P_M \cdot (1 \pm \varepsilon)$, it is possible to calculate the relative deviation Δp_M of the power $P_M^{(array)}$ with reference to the product $N_m \cdot P_M$ (that is, the rated power of the array). Hence, a negative deviation means a lack of maximum power with regard to the rated power of the array. The global index Δp_M is a consequence of both production tolerance and $I–V$ mismatch, i.e.,

$$\Delta p_M = \frac{P_M^{(array)} - N_m \cdot P_M}{N_m \cdot P_M}. \tag{6}$$
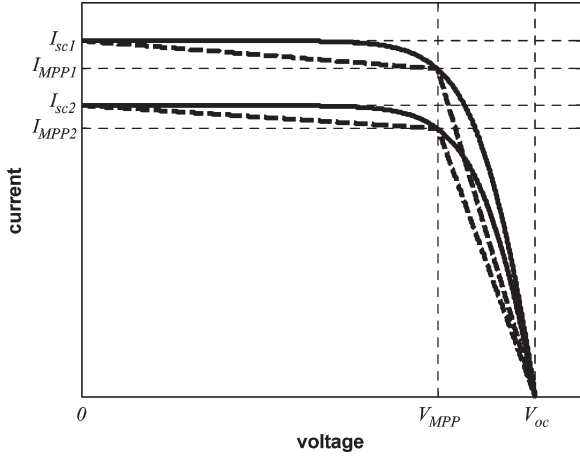
Fig. 2. I–V characteristics of two modules with opposite current mismatch.

A. Series-Connection Mismatch

By examining the series connection of two PV modules equipped with bypass diodes, the worst case in terms of mismatch losses is related to a string of two modules with powers at the opposite limits of tolerance ε in per unit. Thus, the maximum powers are $P_{M1} = P_M \cdot (1 + \varepsilon)$ and $P_{M2} = P_M \cdot (1 - \varepsilon)$. The expected string power is $2 \cdot P_M$, whereas the parameters ℓ_{mis} and Δp_M have the same magnitude.

If the I–V mismatch is considered to be related only to the current (thus, the tolerance ε is valid also for the current parameters), the following equations can be written:

$$V_{\text{oc1}} = V_{\text{oc2}} = V_{\text{oc}} \tag{7}$$

$$V_{\text{MPP1}} = V_{\text{MPP2}} = V_{\text{MPP}} \tag{8}$$

$$I_{\text{MPP1}} = I_{\text{MPP}} \cdot (1 + \varepsilon) \tag{9}$$

$$I_{\text{MPP2}} = I_{\text{MPP}} \cdot (1 - \varepsilon). \tag{10}$$

By maintaining the ratio $I_{\text{MPP}}/I_{\text{sc}}$ constant, similar formulas can be written for the short-circuit currents. Both the piecewise linear approximation (dashed line) and the fully nonlinear model (solid line) of the I–V curve are shown in Fig. 2 for the two modules before the connection. Then, being the modules equipped with bypass diodes, the string characteristics I–V and P–V after the connection are shown in Fig. 3. The power curve exhibits a local MPP at a voltage that is almost equal to V_{MPP}.

With reference to the piecewise linear approximation, simple formulas can be written for voltages, power, and mismatch losses. In particular, the current corresponding to the maximum power of the string is equal to the current of the module with the lower power

$$I_{\text{MPP}}^{(\text{string})} = I_{\text{MPP2}}. \tag{11}$$

The corresponding module voltages are

$$V_1 = V_{\text{MPP}} + \frac{V_{\text{oc}} - V_{\text{MPP}}}{I_{\text{MPP1}}} \cdot (I_{\text{MPP1}} - I_{\text{MPP2}}) \tag{12}$$
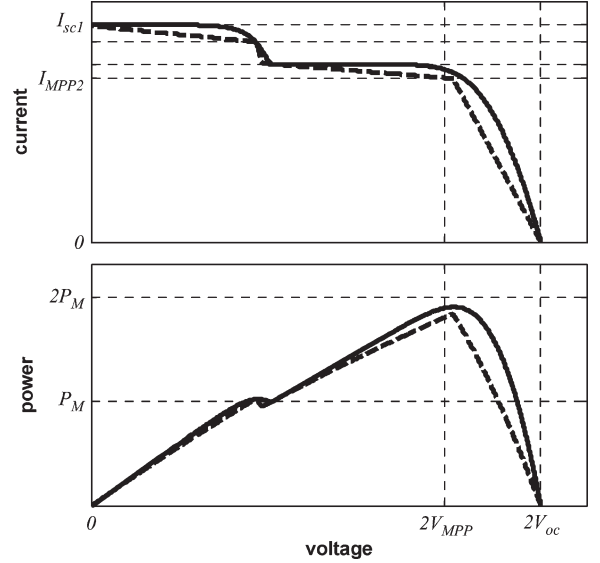
$$V_2 = V_{\text{MPP}} \tag{13}$$

Fig. 3. I–V and P–V string characteristics.

and the maximum power of the string is

$$P_M^{(\text{string})} = 2P_M + 2\varepsilon \cdot \frac{I_{\text{MPP}} \cdot (V_{\text{oc}} - V_{\text{MPP}})}{1 + \varepsilon} - 2\varepsilon P_M - \frac{2\varepsilon^2 I_{\text{MPP}} \cdot (V_{\text{oc}} - V_{\text{MPP}})}{1 + \varepsilon}. \tag{14}$$

Then, the mismatch losses are derived as

$$L_{\text{mis}}^{(\text{string})} = 2P_M - P_M^{(\text{string})}$$
$$= \frac{I_{\text{MPP}} \cdot (2\varepsilon^2 - 2\varepsilon) \cdot (V_{\text{oc}} - V_{\text{MPP}})}{1 + \varepsilon} + 2\varepsilon P_M. \tag{15}$$

Dividing (15) by the expected maximum power of the string $2P_M$, one obtains

$$\ell_{\text{mis}}^{(\text{string})} = \frac{L_{\text{mis}}^{(\text{string})}}{2P_M} = \varepsilon - \mu\varepsilon\frac{1 - \varepsilon}{1 + \varepsilon} \tag{16}$$

where

$$\mu = \frac{V_{\text{oc}}}{V_{\text{MPP}}} - 1. \tag{17}$$

Typical values of μ lie within the range 0.2–0.45 for all the silicon technologies.

From (16), it is possible to draw the mismatch losses as function of the tolerance with piecewise linear approximation (in this case, we assume $\mu = 0.274$ for polycrystalline modules).

It can be stressed that, in Fig. 4, which shows the cases that are valid for two series connected modules, the piecewise linear approximation is very pessimistic, and, with the fully nonlinear model, the rise of $\ell_{\text{mis}}^{(\text{string})}$, when the tolerance increases, is much slower.

Then, the study by fully nonlinear model continues with the case of three or more series-connected modules. With three modules, besides the two modules at the opposite tolerance limits, the third module could lie between $P_M \cdot (1 - \varepsilon)$ and $P_M \cdot (1 + \varepsilon)$, but it is clear that the maximum losses occur
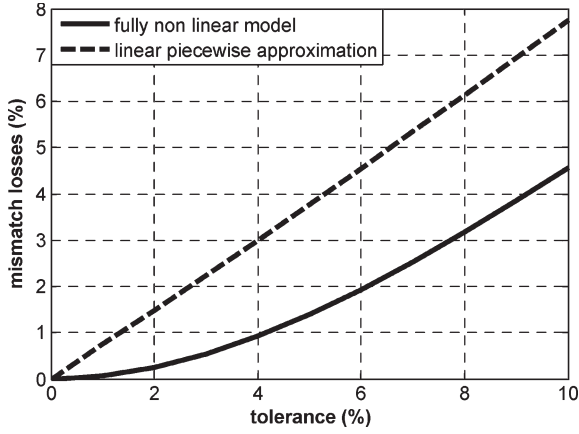
Fig. 4. Mismatch variation of two series-connected modules.

TABLE I
MISMATCH LOSSES FOR THREE SERIES-CONNECTED MODULES

Power of the 3$^{\text{rd}}$ module	Mismatch losses	
	$\varepsilon = 10\,\%$	$\varepsilon = 5\%$
$P_M \cdot (1 + \varepsilon)$	5.4 %	1.5 %
$P_M \cdot (1 - \varepsilon)$	3.4 %	1.1 %
P_M	3.7 %	1.0 %

when the third module has power equal to the maximum limit (Table I with three different values for the third module).

A suitable simulation gives the mismatch losses in a string composed of series-connected modules. In this simulation, the number of modules N_S is constant, but the number of modules with power at maximum tolerance limit N_{S1} is variable, and the remaining modules $N_S - N_{S1}$ have power at minimum tolerance limit. According to (12)–(17) which employ the piecewise linear approximation, the string mismatch is

$$\ell_{\text{mis}}^{(\text{string})} = \frac{\frac{N_{S1}}{N_S}\left(2\varepsilon - 2\mu\varepsilon\frac{1-\varepsilon}{1+\varepsilon}\right)}{2\varepsilon\frac{N_{S1}}{N_S} - \varepsilon + 1} \qquad (18)$$

when the current at MPP is the lowest value.

By varying mutually the number of modules of the two types, it is possible to deduce that the mismatch losses have a peak value (due to the full-model nonlinearity) when the number of modules at maximum limit is about 80% versus 20% at minimum limit for 10% tolerance (about 70% versus 30% for 5% tolerance, Fig. 5). This value is higher than the one corresponding to the two-module connection. The relative deviation Δp_M with more than two modules is different from the mismatch losses $\ell_{\text{mis}}^{(\text{string})}$ because the sum of the maximum powers $P_M^{(i)}$ is different with respect to the product $N_S \cdot P_M$.

The mismatch variation presents a discontinuity around 95% of modules at the maximum power limit (for 10% tolerance), when the current corresponding to the MPP of the string becomes close to the highest MPP current. In this condition, (18) has to be rewritten as

$$\ell_{\text{mis}}^{(\text{string})} = 1 - \frac{\frac{N_{S1}}{N_S}(1+\varepsilon)}{2\varepsilon\frac{N_{S1}}{N_S} - \varepsilon + 1} \qquad (19)$$
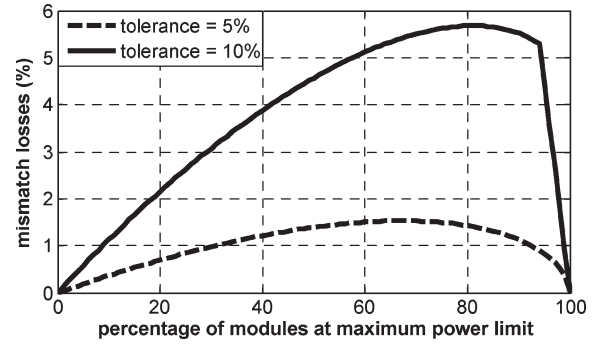
for N_{S1} close to N_S.

Fig. 5. Mismatch variation in series-connected modules.

Equations (18) and (19) are not dependent on the total number of the modules but only on the ratio N_{S1}/N_S.

B. Parallel-Connection Mismatch

For a parallel connection of two strings that are equipped with blocking diodes, we assume that the *I–V* mismatch is essentially limited to voltage (thus, tolerance ε is valid for both power and voltage parameters). Then, the following expressions can be written:

$$I_{\text{sc1}} = I_{\text{sc2}} = I_{\text{sc}} \qquad (20)$$
$$I_{\text{MPP1}} = I_{\text{MPP2}} = I_{\text{MPP}} \qquad (21)$$
$$V_{\text{MPP1}} = V_{\text{MPP}} \cdot (1 + \varepsilon) \qquad (22)$$
$$V_{\text{MPP2}} = V_{\text{MPP}} \cdot (1 - \varepsilon) \qquad (23)$$

and maintaining the ratio $V_{\text{MPP}}/V_{\text{oc}}$ constant, formulas (structurally) dual with respect to the ones presented in Section III-A can be written for the open circuit voltages.

With piecewise linear approximation, a simple equation can be written for the mismatch losses

$$\ell_{\text{mis}}^{(\text{array})} = \frac{L_{\text{mis}}^{(\text{array})}}{2P_M} = \varepsilon - \lambda\varepsilon\frac{1-\varepsilon}{1+\varepsilon} \qquad (24)$$

where

$$\lambda = \frac{I_{\text{sc}}}{I_{\text{MPP}}} - 1. \qquad (25)$$

Typical values of λ are within the range 0.06–0.3 for all the silicon technologies. As a practical example, a value of 0.09 is employed for p-Si technology.

Fig. 6 shows the *I–V* characteristics of two strings having a voltage mismatch.

The array *I–V* and *P–V* curves are plotted in Fig. 7, in which the gain due to the blocking action of the diodes is evident near the open-circuit voltage. Yet, the piecewise linear approximation is very pessimistic, while the fully nonlinear model gives mismatch losses with very slow rise ($\ell_{\text{mis}}^{(\text{array})} \approx 5\%$ with tolerance of 10%, as shown in Fig. 8).

Now, we consider the situation of three strings as with the previous study: the worst case is always with one string with power at minimum limit and the other two at maximum limit (Table II).

Then, by increasing the number of parallel-connected strings to simulate the increase of the array power, the number of
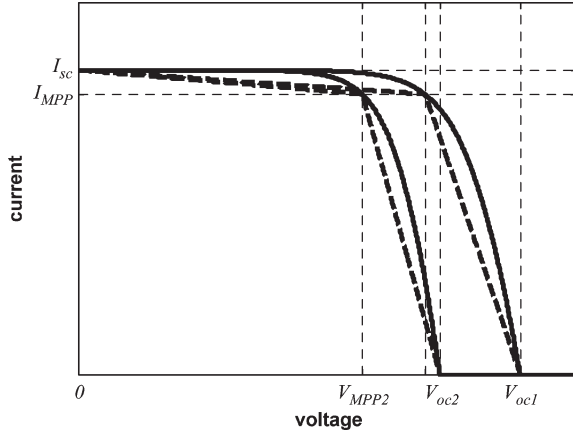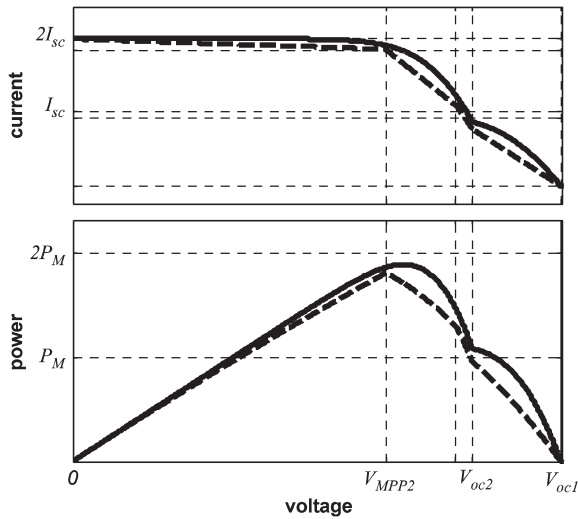
Fig. 6.   String I–V characteristics with voltage mismatch.

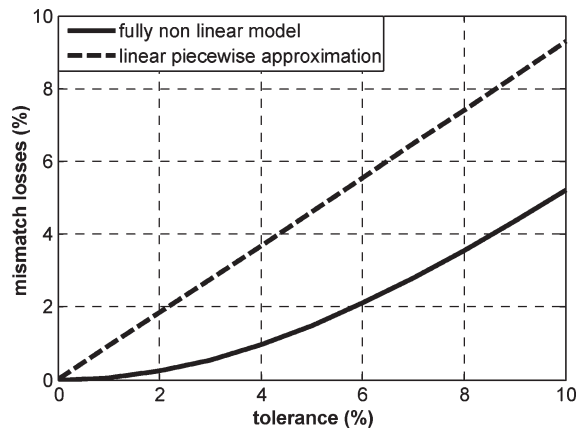Fig. 7.   Two parallel-connected-string characteristics.

Fig. 8.   Mismatch variation of two parallel-connected strings.

strings N_P is maintained constant, but the number of strings at maximum power limit N_{P1} is increased progressively. The peak values of mismatch losses occur at about 70% of the strings at maximum for 10% tolerance (about 60% for 5% tolerance, Fig. 9). In this case, the relative deviation Δp_M is different from the mismatch losses $\ell_{\mathrm{mis}}^{(\mathrm{array})}$. Again, the maximum value with more strings is higher than the value corresponding

TABLE II
MISMATCH LOSSES FOR THREE PARALLEL-CONNECTED STRINGS

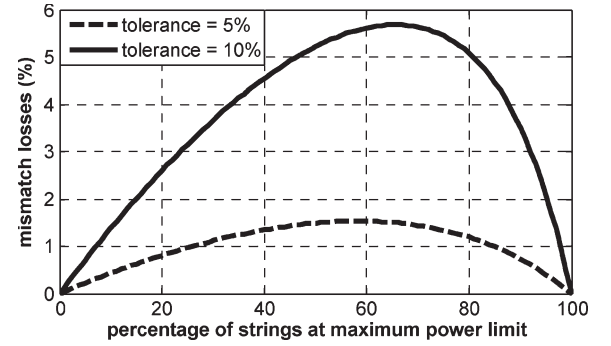| Power of the 3$^{\mathrm{rd}}$ string	Mismatch losses	
	$\varepsilon = 10\%$	$\varepsilon = 5\%$
$P_M \cdot (1 + \varepsilon)$	5.7 %	1.5 %
$P_M \cdot (1 - \varepsilon)$	3.5 %	1.2 %
P_M	3.8 %	1.0 %

Fig. 9.   Mismatch variation in parallel-connected strings.

TABLE III
STRING CONFIGURATIONS AND THE CORRESPONDING MISMATCH

modules	P_{max}	Mismatch losses	
		$\varepsilon = 10\%$	$\varepsilon = 5\%$
1 – 2	$2P_M$	4.6 %	1.4 %
1 – 3	$2P_M \cdot (1 + \varepsilon)$	1.2 %	0.36 %
1 – 4	$2P_M$	1.3 %	0.36 %
2 – 3	$2P_M$	1.6 %	0.40 %
2 – 4	$2P_M \cdot (1 - \varepsilon)$	1.5 %	0.40 %
3 – 4	$2P_M$	0 %	0 %

to only two strings. Similar to the series-connection mismatch, (18) and (19) can be written here by changing N_S, N_{S1}, μ, and $\ell_{\mathrm{mis}}^{(\mathrm{string})}$ in N_P, N_{P1}, λ, and $\ell_{\mathrm{mis}}^{(\mathrm{array})}$, respectively.

C. Series-Parallel-Connection Mismatch

In order to evaluate the I–V mismatch in a PV array, the simplest connection of two parallel strings of two series modules is analyzed. Hence, two modules have current mismatch (labeled #1 and #2), as occur in (7)–(10), whereas the other two have voltage mismatch (#3 and #4), as supposed in (20)–(23). The rated power of the array is $4P_M$, and, thus, the mismatch losses and relative deviation coincide.

First, the possible configurations of the strings are simulated and clearly, the highest mismatch losses happen with modules #1 and #2, while no mismatch losses occur with modules #3 and #4 (Table III).

Then, the three possible combinations of the strings in the array are studied (Table IV), and the mismatch losses of the array are intermediate with respect to the values of the strings. The worst case occurs with a module with current mismatch connected to a module with voltage mismatch. The maximum amount of mismatch losses is 3.3% for the 10% tolerance and 0.80% for the 5% tolerance.

TABLE IV
ARRAY CONFIGURATIONS AND THE RELATED MISMATCH

combination		$\varepsilon = 10\%$	$\varepsilon = 5\%$
$1-2$	$3-4$	2.4%	0.71%
$1-3$	$2-4$	3.1%	0.79%
$1-4$	$2-3$	3.3%	0.80%

IV. REVERSE-CURRENT ESTIMATION

Let us consider N_p identical strings connected in parallel in open-circuit conditions without blocking diodes, due, for example, to a shut down of the dc–ac converter. If one of these strings is subjected to zero irradiance (total shading without diffuse irradiance), a reverse current will be generated into itself. It can be pointed out that this is the worst case and very uncommon in practice. For the Kirchhoff's current law, the current generated by the $N_p - 1$ "normally irradiated" strings must be equal to the reverse current flowing into the passive string.

By the piecewise linear approximation, the equation of the normally irradiated strings is, according to the Thévenin's theorem

$$V = V_{\text{oc}} - \frac{R_i}{N_p - 1} I \qquad (26)$$

where R_i has been defined in Section II.

In the passive string, there are two contributions to voltage, both positive

$$V = V_{\text{MPP}} + R_i \cdot (I - I_{\text{sc}} + I_{\text{MPP}}). \qquad (27)$$

Solving (26) and (27) and considering (4), for $I = I_{\text{rev}}$ and $V = V_o$, one obtains

$$I_{\text{rev}} = I_{\text{sc}} \frac{N_p - 1}{N_p} \qquad (28)$$

$$V_o = V_{\text{oc}} - \frac{V_{\text{oc}} - V_{\text{MPP}}}{N_p} \cdot \frac{I_{\text{sc}}}{I_{\text{MPP}}}. \qquad (29)$$

Due to the "horizontal" symmetry between the $I–V$ characteristics of an irradiated string and a totally shaded string and to the "linearity" of the last part close to the open-circuit point (Fig. 10), the piecewise linear approximation and the fully nonlinear model provide the same reverse current, even if the linear approximation gives an underestimation of the resulting open-circuit voltage.

If we give a major generality to the discussion, increasing the number of parallel-connected strings with one string completely passive, the reverse current grows up to an asymptote equal to the short-circuit current of one string (Fig. 11).

By using the piecewise linear approximation, in case of N_p parallel strings without blocking diode, if one of them is passive (totally shaded), the current corresponding to the MPP voltage decreases down to

$$I_{V_{\text{MPP}}} = (N_p - 1) \cdot I_{\text{MPP}} - (I_{\text{sc}} - I_{\text{MPP}}) = N_p \cdot I_{\text{MPP}} - I_{\text{sc}} \qquad (30)$$

and the array maximum power is about

$$P_M^{(\text{array})} \cong (N_p - 1 - \lambda) \cdot P_M^{(\text{string})} \qquad (31)$$
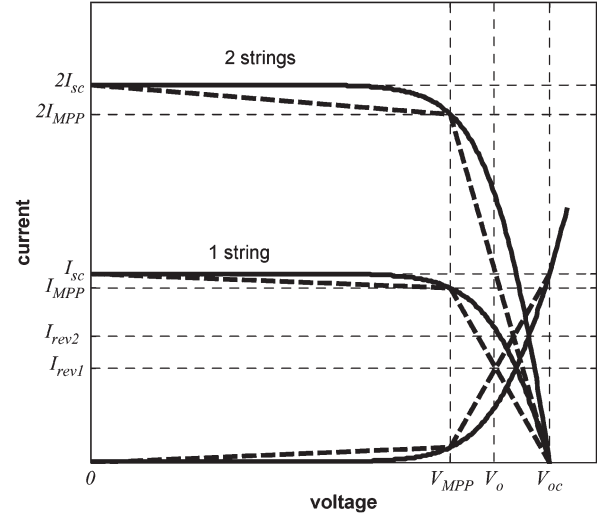

Fig. 10. Reverse current in a zero-irradiance string.
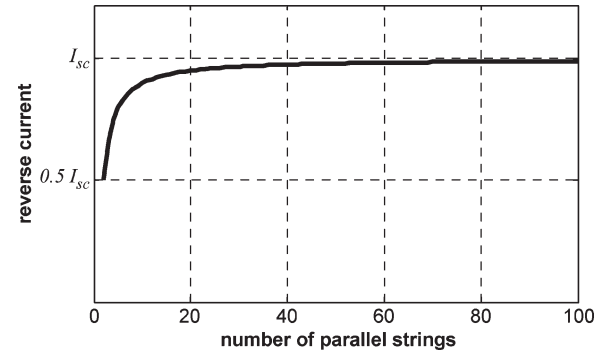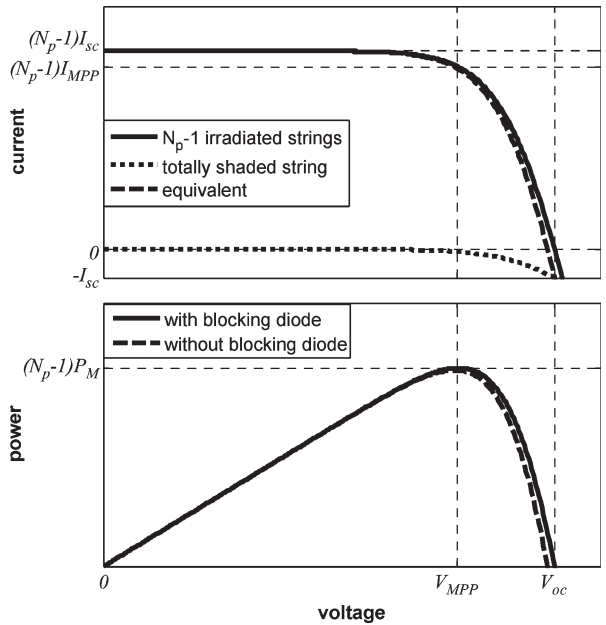

Fig. 11. Variation of reverse current.

Fig. 12. Effect of blocking diodes.

with λ already defined in (25). The use of the blocking diode permits the improvement of the power performance, as can be seen in Fig. 12.
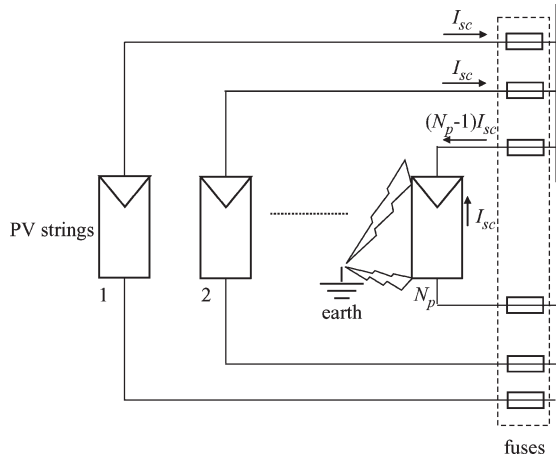
Fig. 13.   Short-circuit and fuse protection.

Nevertheless, another concern can be a reverse current in the string cables (not in the modules): the largest amount of stress is determined by two earth faults within the PV array. In this case, the current can become $(N_p - 1)$ times the short-circuit current of the module, and the designer can choose fuses as overcurrent protection (Fig. 13). However, for PV modules with protection class II (double isolation), possible earth faults are not an issue [21]. Currently, most PV modules have double isolation.

Finally, there are some conditions under which the use of blocking diodes and/or fuses which prevent reverse flow of current can be avoided.

1) Double isolation of PV modules is required.
2) PV modules must accept current in the reverse direction up to, at least, the short-circuit current (some manufacturers give twice this amount).
3) The bypass diodes in the junction box of every PV module must be short-circuit proof.
4) All cables must be in double isolation; this applies to cables connecting a module with the previous and the next one provided by module manufacturers, as well as to cables from poles of every string to the input of the dc–ac converter.

Double isolation makes the probability of earth failure negligible. The isolation test within International Electrotechnical Commission (IEC) certification is carried out at the beginning of the tests of accelerated aging [22]. Nevertheless, it should be carried out also at the end of the tests, in such a way as to guarantee the double isolation up to 25 years of operation.

V. STUDY CASES

In this section, the main simulation results, concerning I–V mismatch losses and reverse current, are presented with reference to practical systems of 2 MW and 20 kW, respectively. The start point is the database of flash test on every PV module. However, the flash reports are available without the indication of the uncertainty of measurement which can exceed ±4% in commercial sun simulators.

In the 2-MW system, the p-Si technology with directional solidification has been used. The modules P-220 have rated power

TABLE V
MODULE ELECTRIC PARAMETERS

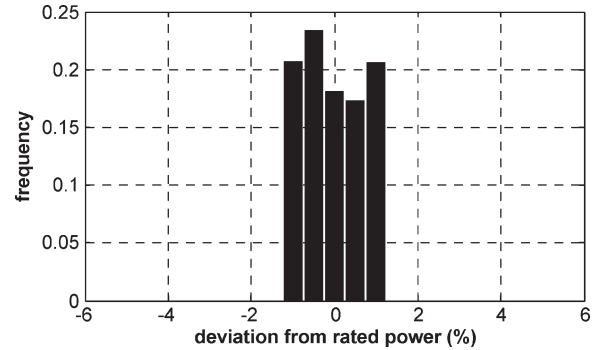| Parameters	PV module type	
	P-220	I-165
Rated voltage V_{MPP} [V]	28.5	17.4
Rated current I_{MPP} [A]	7.55	9.48
Open circuit voltage V_{oc} [V]	36.3	21.6
Short circuit current I_{sc} [A]	8.20	10.14
Rated power P_M [W]	215±3%	165±10%

Fig. 14.   Power dispersion of P-220 modules.

$P_M = 215$ W with 60 square cells of 156-mm side (efficiency 13%). The power tolerance is ±3% (recent modules).

In the 20-kW system, the m-Si Czochralski technology has been employed. Every module I-165 consists of 108 pseudo-square cells of 103-mm side (efficiency 13%) with rated power $P_M = 165$ W. The power tolerance is ±10% (production is some years ago).

Table V presents the rated parameters of the modules used for the two plants. Both systems are equipped with blocking diodes and fuses for each string (and for each group of eight strings in the 2-MW system) against reverse currents.

A. 2-MW System With P-220 Multicrystalline Silicon Modules

The modules are arranged in eight arrays with about 250 kW each. All the strings include 16 series-connected modules. Four arrays are composed of 72 strings and four arrays are composed of 73 strings. The global number of modules is 9280.

In a sample of 4600 modules, which is equal to about 50% of the population, the distribution of occurrences of the module power is very regular (Fig. 14). The mean value of the module maximum power is 214.9 W, denoting a power deviation of about −0.03% with respect to the rated value (lack of power). Moreover, if we consider the parameters open-circuit voltage V_{oc}, short-circuit current I_{sc}, and the corresponding current I_{MPP} and voltage V_{MPP} at the MPP, the distributions are similar to the reference Gaussian. Only the mean values of the current parameters I_{sc} and I_{MPP} are biased around −2%, −1% (lack of current) with respect to the rated values.

Therefore, from the flash reports, the actual fill factor of the run production seems very close to the declared value, which is measured in "qualification and type approval" phase on a little sample of modules [22] (Fig. 15).
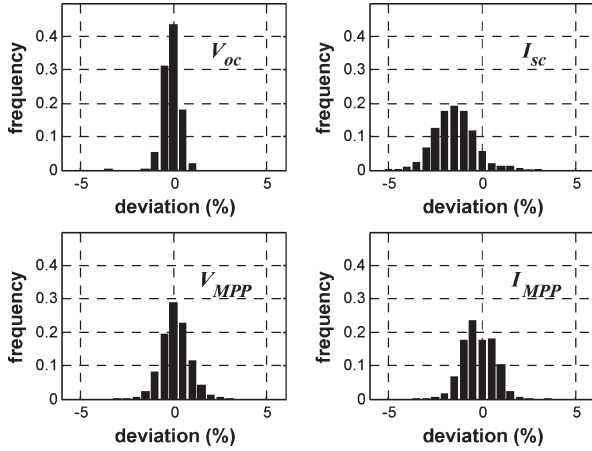
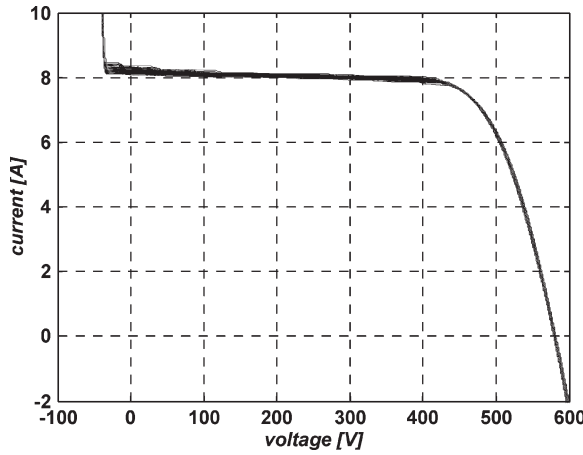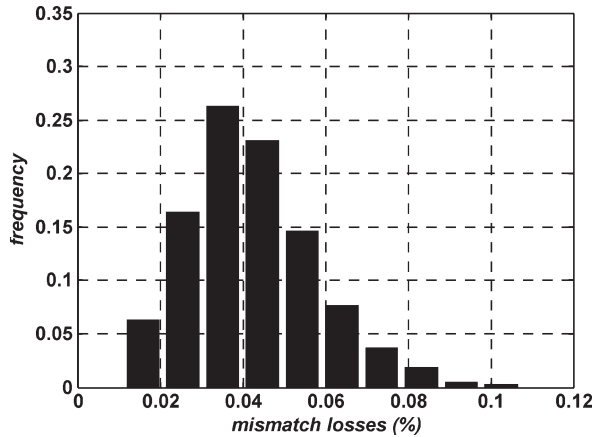Fig. 15. Electric-parameter dispersion of P-220 modules.

Fig. 16. Mismatch of 1000 I–V string characteristics (P-220).

Fig. 17. Mismatch losses (P-220) for 1000 strings.

The position of each module, according to its serial number, in a single array is unknown, and, thus, a random algorithm has been used to generate the configuration of modules in one array.

Now, by continuing the analysis with series connection of modules in the strings, it is possible to obtain the string I–V characteristics and the corresponding distributions of mismatch losses $\ell_{\mathrm{mis}}^{(\mathrm{string})}$ and power deviation $\Delta p_M^{(\mathrm{string})}$ (Figs. 16–18) for 1000 strings composed by a random choice of modules.
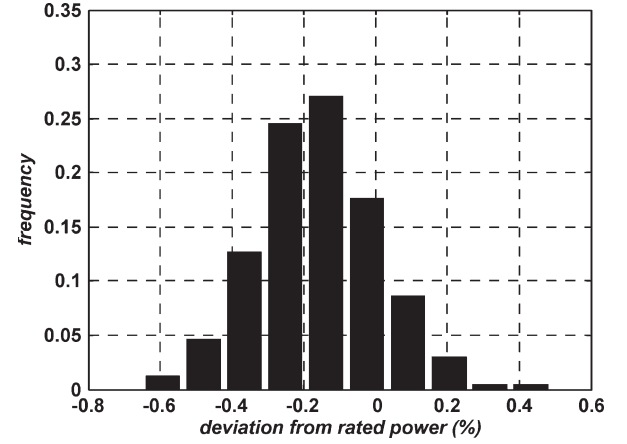

Fig. 18. String power deviation (P-220).

TABLE VI
P-220 SIMULATION RESULTS

Rated power $N_m \cdot P_m$	247.68 kW
Module power $\sum P_M^{(i)}$	247.60 kW
Actual power $P_M^{(array)}$	246.17 kW
Mismatch $\ell_{mis}^{(array)}$	0.57 %
Deviation Δp_M	-0.61 %

The mode and the maximum value of mismatch losses $\ell_{\mathrm{mis}}^{(\mathrm{string})}$ are about 0.035% and 0.11%, respectively, while the mode and the maximum value of power deviation $\Delta p_M^{(\mathrm{string})}$ are around -0.15% and -0.6%, respectively, in terms of lack of power.

Finally, after the connection of 72 strings, the mismatch losses and the power deviation of one array are presented in Table VI, taking into account the power losses of blocking diodes. It can be stressed that, although the string-mismatch losses are very low, the array mismatch is higher due to voltage mismatch in the strings.

According to the high number of parallel strings in each array (72 or 73), the reverse current flowing in a totally shaded string (zero irradiance) is close to the short-circuit current of one module.

B. 20-kW System With I-165 Monocrystalline Silicon

In the population of 120 modules, the distribution of frequencies is very irregular, with mode around -1.6% (lack of power). Then, the fill factor of the modules is clearly lower than the declared value which is referred to a little sample of the run production. Open-circuit voltage, short-circuit current, and current at maximum power are higher than the declared values, whereas the voltage at MPP is lower than declared (Figs. 19 and 20). That means that the material of run production is substantially different from the sample which is tested in the "qualification and type approval" phase [22].

The array configuration is five strings with 24 series-connected modules. In order to evaluate the string-mismatch losses, 200 strings randomly composed have been studied obtaining the string I–V characteristics (Fig. 21) and the corresponding distributions of mismatch losses $\ell_{\mathrm{mis}}^{(\mathrm{string})}$ centered in
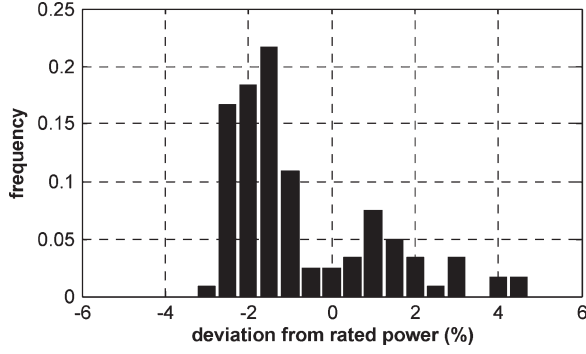
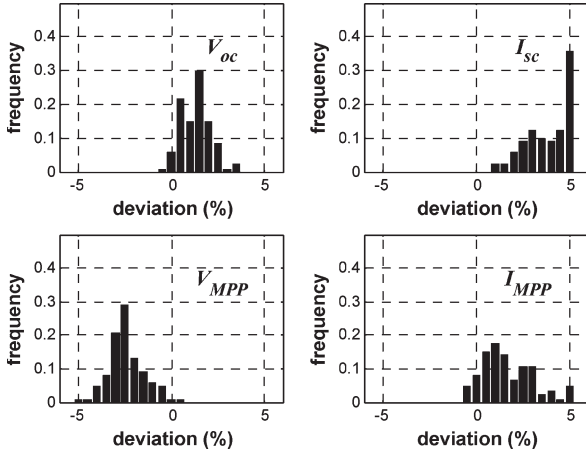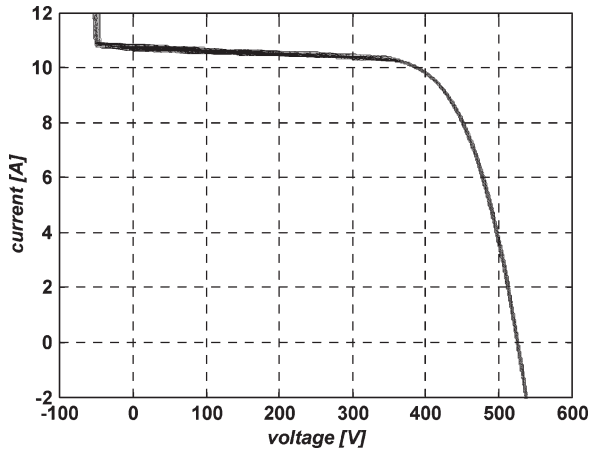Fig. 19.   Power dispersion of I-165 modules.

Fig. 20.   Electric-parameter dispersion of I-165 modules.

Fig. 21.   Mismatch of 200 $I–V$ string characteristics (I-165).

0.1% (Fig. 22) and relative power deviation $\Delta p_M^{(\text{string})}$ centered in -0.9% (Fig. 23).

Finally, after connection of the five strings, the mismatch losses and the power deviation of the array are presented in Table VII, taking into account the losses of blocking diodes.

VI. EXPERIMENTAL RESULTS ON OPERATING SYSTEMS

The testing on a PV array to obtain $P_M^{(\text{array})}$ requires the measurement of the $I–V$ characteristics at natural sunlight through midday hours. Calibrated solar cells (in p-Si and m-Si,
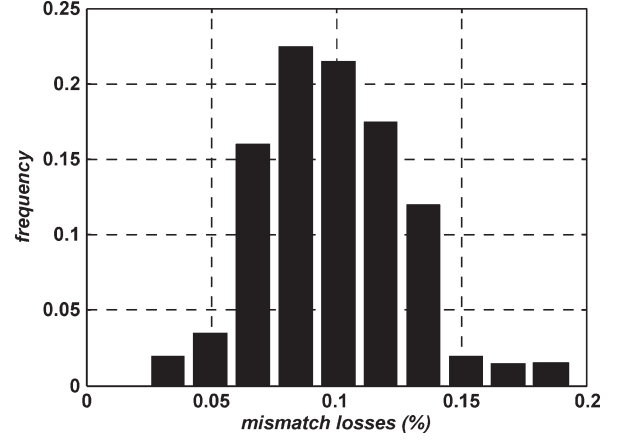

Fig. 22.   Mismatch-losses deviation (I-165).
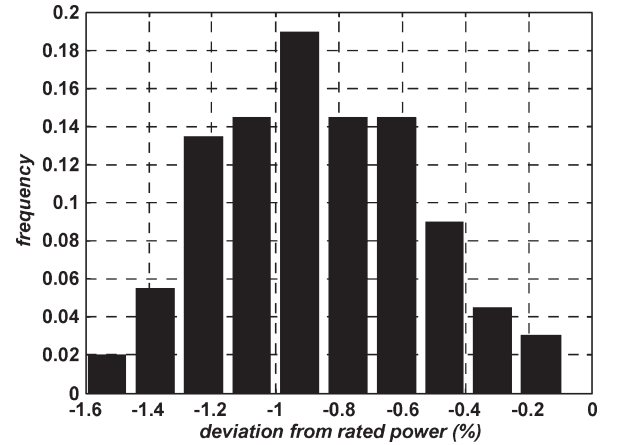
Fig. 23.   String-power deviation (I-165).

TABLE VII
I-165 SIMULATION RESULTS

Rated power $N_m \cdot P_m$	19.80 kW
Module power $\sum P_M^{(i)}$	19.64 kW
Actual power $P_M^{(array)}$	19.54 kW
Mismatch $\ell_{mis}^{(array)}$	0.56 %
Deviation Δp_M	-1.33 %

respectively) are used as irradiance sensors to take into account the spectral losses. Each $I–V$ characteristic is obtained, in a single sweep, by the transient charge of a suitable capacitor, with high capacitance (e.g., 1–10 mF) with regard to the equivalent capacitance of the solar cells in the array. This method is better, for cost and size reasons, than the electronic-load method when voltage is higher than 100 V and current is higher than 10 A.

The measured $I–V$ characteristics have to be extrapolated to the STC, according to the method of the IEC standard [22], [23] in order to determine the actual power $P_M^{(\text{array})}$.

The involved equations, referred to a single module, are

$$I_2 = I_1 + I_{\text{sc1}} \cdot \left(\frac{G_2}{G_1} - 1 \right) + \alpha(T_2 - T_1) \tag{32}$$

$$V_2 = V_1 - R_S \cdot (I_2 - I_1) - K I_2 \cdot (T_2 - T_1) + \beta(T_2 - T_1) \tag{33}$$

TABLE VIII
MEASUREMENT UNCERTAINTIES

G	T_c	V_{oc}	I_{sc}	$P_M^{(array)}$	$P_M^{(array)}$@STC
$\pm 2.5\,\%$	$\pm 2\,°C$	$\pm 0{,}1\,\%$	$\pm 1\,\%$	$\pm 1{,}1\,\%$	$\pm 4\,\%$

where the subscripts 1 and 2 correspond to the actual measurement conditions and the standard conditions, respectively; moreover α and β are the temperature coefficients of I_{sc} and V_{oc}, respectively, R_S is the series resistance, and K is a curve correction factor.

The PV array testing tells us how much the maximum power $P_M^{(array)}$, within the measurement uncertainty (Table VIII), is close to the nameplate data. Furthermore, the nameplate data must be reduced by an amount due to the following [26]:

1) I–V mismatch and consequent power deviation according to flash tests;
2) negligible glass reflection, since the beam is almost normal (840–1100 W/m^2), and small soiling impact after dirt removal consequent to rain in the day preceding the measurements (about 2%) [27];
3) losses in dc cabling, blocking diodes, and fuses, evaluated taking into account the length and the section of wires, the voltage drop on diodes, and fuses (about 2%).

Note that the method of conversion to STC is as much accurate as the irradiance and the temperature are close to STC, as it occurs in our measurements $G = 840$–1100 W/m^2 and $T_c = 34\,°C$–$41\,°C$. Therefore, the conversion error can be considered to be negligible. The measurements have been carried out in mid-September. On the PV site, the sun height was higher than $50°$ and the tilt angle of the PV module is $30°$; therefore, the angle of the beam with respect to the direction normal to the glass is less than $10°$.

All the measurements are carried out by an Automatic Data Acquisition Systems (ADAS) described in [25]. The main performance of the measurement includes: resolution of 12 b and maximum sampling rate of 500 kS/s with single channel and lower sampling rate with a multiplexer for multichannel acquisition. A suitable BNC connector enables the use of differential probes 200:1 and current clamps with various sensitivities as, for example, 1–100 mV/A. Owing to the proper software implemented in Labview, ADAS behaves as a storage oscilloscope for the measurement of voltage (up to 1000 V$_{pk}$), current (up to 2000 A$_{pk}$). The oscilloscope, in order to obtain the I–V curves of the PV arrays, is equipped with a trigger system, which is useful for the capture of the transient charge of a capacitor. Our ADAS is periodically checked in the calibration laboratory for adjusting both the attenuation ratio of the differential probes and the sensitivity of the current clamps.

The experimental results, concerning practical arrays with 2 MW and 20 kW powers, show a sensible difference with respect to the simulations carried out on the basis of the flash reports.

Table IX shows the experimental results concerning the 2-MW system. Note that the measured irradiance and temperature are close to the values of STC. These results are summarized in Table X, highlighting remarkable deviations from the rated power. The reason is mainly due to an excessive voltage drop, as can be seen in the ratio $V_{MPP}/V_{oc} = 0.70 \div 0.74$. In this case, both blocking diodes and fuses are used: thus, several ones are operating in abnormal conditions. Only array # 6 with 73 strings has a deviation of less than 10% with an almost normal value of the ratio $V_{MPP}/V_{oc} = 0.76$. The deviation of 7.6% is considered in comparison with the rated values corrected by the previous global amount of about 4%. The conclusion is that the practical deviation in on-site operation is at least 3%–4% (within the measurement uncertainties of sun simulators and our ADAS).

Qualitatively, similar results have been obtained with the modules of the 20-kW system.

Fig. 24 compares the measured I–V and P–V characteristics with respect to the STC for array #6.

The reverse current is avoided by the blocking diodes. However, if the open-circuit voltages are considered, a voltage mismatch of 2% exists among the arrays. Thus, with more than 70 parallel strings and without shading effect, the reverse current in the worst string in open-circuit conditions would be less than 1 A. In the case of one string subjected to zero irradiance working in passive mode, the reverse current I_{rev} generated by the remaining irradiated strings is about 8 A.

VII. CONCLUDING REMARKS

On-site measurements have proven that flash reports with unknown measurement uncertainty could present an optimistic situation with regard to I–V mismatch and deviation from the rated power.

It is worth noting that, in actual conditions during outdoor operation, the solar irradiance is uniform (parallel beams), the solar spectrum is different from the reference one AM = 1.5, and the rows of structures which support the modules can be slightly out of alignment.

However, for the flash reports in STC, the sun simulator cannot provide totally uniform irradiance with portions subjected to different values of irradiance, particularly in current modules with surface higher than 1.5 m^2. The analysis of some sun-simulator specifications proves that the uniformity errors are between $\pm 1\%$ and $\pm 4\%$; furthermore, the stability during the lamp pulse cannot be better than $\pm 1\%$.

Therefore, the rated values, given without measurement uncertainty, can be overestimated up to 3%–4% with respect to the on-site measurements.

Finally, the simulation results reveal that the impact of manufacturing I–V mismatch is negligible with the usual tolerance, while the insertion of blocking diodes and fuses against reverse currents can be avoided if the specific conditions presented in Section IV are satisfied. In these conditions, fuses are not useful to avoid reverse current in the modules, as the maximum reverse current is less than the short-circuit current. In any case, it is not advisable to insert both devices (blocking diodes and fuses).

TABLE IX
ON-SITE MEASUREMENT RESULTS

Parameters	Arrays with 72 strings				Arrays with 73 strings			
	#1	#2	#3	#4	#5	#6	#7	#8
G [W/m^2]	1105	993	924	862	1063	961	928	838
T_c [°C]	34.0	36.7	41.3	38.2	33.9	32.5	40.9	38.5
P_M [kW]	228.0	203.2	190.4	181.2	219.2	216.4	189.2	162.1
V_{MPP}[V]	395.41	396.01	394.32	400.96	395.66	430.42	394.64	407.12
I_{MPP}[A]	576.7	513.0	483.0	451.9	554.0	502.8	479.5	398.2
V_{oc}[V]	566.55	556.90	545.67	550.07	564.37	564.77	543.54	548.92
I_{sc}[A]	651.3	567.4	531.8	498.7	614.8	553.7	537.2	436.9
FF	61.8%	64.3%	65.6%	66.0%	63.2%	69.2%	64.8%	67.6%
V_{MPP}/V_{oc}	0.70	0.71	0.72	0.73	0.70	0.76	0.73	0.74
I_{MPP}/I_{sc}	0.88	0.90	0.91	0.91	0.90	0.91	0.89	0.91
P_M@ STC [kW]	221.7	217.0	220.9	218.7	219.1	232.0	217.9	200.5
V_{MPP}@ STC [V]	421.03	419.35	422.29	414.14	424.97	445.23	418.99	422.60
I_{MPP}@ STC [A]	526.5	517.5	523.1	528.1	515.6	521.2	520.1	474.4

TABLE X
2-MW-SYSTEM POWER DEVIATION

Parameters	Arrays with 72 strings				Arrays with 73 strings			
	#1[i]	#2	#3	#4	#5	#6	#7[ii]	#8[iii]
Rated power [kW]	253.4	247.7	247.7	247.7	251.1	251.1	245.3	227.0
$P_M^{(array)}$ [kW]	221.7	217.0	220.9	218.7	219.1	232.0	217.9	200.5
Δp_M (%)	-12.5	-12.4	-10.8	-11.7	-12.8	-7.6	-11.2	-11.7

i. with 220 W modules
ii. with 210 W modules
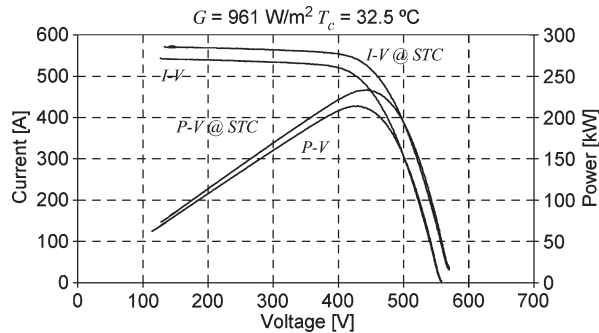iii. the reduction of the rated power is due to the failure of one string-box fuse

Fig. 24. I–V and P–V characteristics in actual conditions and in STC.

REFERENCES

[1] A. Ristow, M. Begovic, A. Pregelj, and A. Rohatgi, "Development of a methodology for improving photovoltaic inverter reliability," *IEEE Trans. Ind. Electron.*, vol. 55, no. 7, pp. 2581–2592, Jul. 2008.

[2] S. Busquets-Monge, J. Rocabert, P. Rodríguez, S. Alepuz, and J. Bordonau, "Multilevel diode-clamped converter for photovoltaic generators with independent voltage control of each solar array," *IEEE Trans. Ind. Electron.*, vol. 55, no. 7, pp. 2713–2723, Jul. 2008.

[3] G. Carannante, C. Fraddanno, M. Pagano, and L. Piegari, "Experimental performance of MPPT algorithm for photovoltaic sources subject to inhomogeneous insolation," *IEEE Trans. Ind. Electron.*, vol. 56, no. 11, pp. 4374–4380, Nov. 2009.

[4] J. T. Bialasiewicz and E. Muljadi, "RPM-SMA-based modeling of photovoltaic panels as energy sources in renewable energy systems," in *Proc. 28th IEEE IECON*, Nov. 5–8, 2002, vol. 4, pp. 3360–3365.

[5] J. T. Bialasiewicz, "Renewable energy systems with photovoltaic power generators: Operation and modeling," *IEEE Trans. Ind. Electron.*, vol. 55, no. 7, pp. 2752–2758, Jul. 2008.

[6] S. B. Kjaer, J. K. Pedersen, and F. Blaabjerg, "A review of single-phase grid-connected inverters for photovoltaic modules," *IEEE Trans. Ind. Appl.*, vol. 41, no. 5, pp. 1292–1306, Sep./Oct. 2005.

[7] C. Hua, J. Lin, and C. Shen, "Implementation of a DSP-controlled photovoltaic system with peak power tracking," *IEEE Trans. Ind. Electron.*, vol. 45, no. 1, pp. 99–107, Feb. 1998.

[8] E. Roman, R. Alonso, P. Ibanex, S. Elorduizapatarietxe, and D. Goitia, "Intelligent PV module for grid-connected PV systems," *IEEE Trans. Ind. Electron.*, vol. 53, no. 4, pp. 1066–1073, Jun. 2006.

[9] N. D. Kaushika and N. K. Gautam, "Energy yield simulations of interconnected solar PV arrays," *IEEE Trans. Energy Convers.*, vol. 18, no. 1, pp. 127–134, Mar. 2003.

[10] P. A. B. James, A. S. Bahaj, and R. M. Braid, "PV array < 5 kWp + single inverter = grid connected PV system: Are multiple inverter alternatives economic?" *Sol. Energy*, vol. 80, no. 9, pp. 1179–1188, Sep. 2006.

[11] K. F. Teng and P. Wu, "PV module characterization using Q-R decomposition based on the least square method," *IEEE Trans. Ind. Electron.*, vol. 36, no. 1, pp. 71–75, Feb. 1989.

[12] D. Sera, R. Teodorescu, and P. Rodriguez, "PV panel model based on datasheet values," in *Proc. IEEE ISIE*, Jun. 4–7, 2007, pp. 2392–2396.

[13] R. C. Campbell, "A circuit-based photovoltaic array model for power system studies," in *Proc. 39th NAPS*, Sep. 30–Oct. 2, 2007, pp. 97–101.

[14] *Guidelines for the Assessment of Photovoltaic Plants—Initial and Periodic Tests on PV Plants*, Commission Eur. Communities, Joint Res. Centre, Ispra, Italy, 1995.

[15] M. C. Alonso-Garcia, J. M. Ruiz, and F. Chenlo, "Experimental study of mismatch and shading effects in the I–tV characteristics of a photovoltaic module," *Sol. Energy Mater. Sol. Cells*, vol. 90, no. 3, pp. 329–340, Feb. 2006.

[16] E. Karatepe, M. Boztepe, and M. Colak, "Development of a suitable model for characterizing photovoltaic array with shaded solar cells," *Sol. Energy*, vol. 81, no. 8, pp. 977–992, 2007.

[17] K. Wilson, D. De Ceuster, and R. A. Sinton, "Measuring the effect of cell mismatch on module output," in *Proc. 4th IEEE World Conf. Photovoltaic Energy Convers.*, May 2006, vol. 1, pp. 916–919.

[18] J. Bany, J. Appelbaum, and A. Braustein, "The influence of parameter dispersion of electrical cells on the array power out," *IEEE Trans. Electron Devices*, vol. 24, no. 4, pp. 1032–1040, Aug. 1977.

[19] N. D. Kaushika and A. K. Rai, "An investigation of mismatch losses in solar photovoltaic cell networks," *Energy*, vol. 32, no. 5, pp. 755–759, May 2007.

[20] E. Lorenzo, *Solar Electricity: Engineering of Photovoltaic Systems*. Spain: Progensa, 1994.

[21] W. Roth *et al.*, *Photovoltaic Systems*. Freiburg, Germany: Fraunhofer Inst. Solar Energy Syst. ISE, 1995.

[22] *Crystalline Silicon Terrestrial Photovoltaic (PV) Modules. Design Qualification and Type Approval*, IEC 1215, EN 61215: 2005-05, 2006.

[23] *Procedures for Temperature and Irradiance Corrections to Measured I–V Characteristics of Crystalline Silicon PV Devices*, IEC Standard 60891, 1987.

[24] O. Perpiñan, E. Lorenzo, and M. A. Castro, "On the calculation of energy produced by a PV grid-connected system," *Prog. Photovolt., Res. Appl.*, vol. 15, no. 3, pp. 265–274, 2007.

[25] F. Spertino, A. Abete, and R. Napoli, "Experimental testing of grid-connected PV systems with different power in order to assess the yearly energy production," in *Proc. 21st Eur. Photovoltaic Sol. Energy Conf.*, Dresden, Germany, 2006, pp. 2312–2315.

[26] A. H. M. E. Reinders, V. A. P. Van dijk, E. Wiemken, and W. C. Turkenburg, "Technical and economic analysis of grid-connected PV systems by means of simulation," *Prog. Photovolt.*, vol. 7, no. 1, pp. 71–82, 1999.

[27] A. Lloret, J. Andreu, J. Merten, J. Puigdollers, O. Aceves, L. Sabata, M. Chantant, and U. Eicker, "Large grid connected hybrid PV system integrated in a public building," *Prog. Photovolt., Res. Appl.*, vol. 6, pp. 453–464, 1998.

Filippo Spertino (M'07) received the M.Sc. and Ph.D. degrees in electrical engineering from the Politecnico di Torino (PdT), Turin, Italy, in 1995 and 2000, respectively.

He is currently an Assistant Professor of Electric Power Systems and Renewable Energy Systems, Dipartimento di Ingegneria Elettrica, PdT. His research activities include design and simulations, experimental tests, and calibration on photovoltaic and wind-energy systems.

Dr. Spertino is a member of the Institute of Italian Electrical Engineers and the Italian Electrotechnical Committee (CEI).

Jean Sumaili Akilimali received the B.Sc. degree in "Sciences Appliquées (option: Electricité)" from the University of Kinshasa, Kinshasa, Democratic Republic of the Congo, in 1998, and the M.Sc. and Ph.D. degrees in electrical engineering from the Politecnico di Torino (PdT), Turin, Italy, in 2004 and 2008, respectively.

He is currently a Research Assistant in the Dipartimento di Ingegneria Elettrica, PdT. His research activities include distribution systems analysis, distributed generation applications, electricity customers classification, and photovoltaic systems.